Aust. J. Phys., 1984, **37**, 359–87

Pulsed Field Gradient Nuclear Magnetic Resonance as a Probe of Liquid State Molecular Organization*

P. T. Callaghan

Physics Group, Department of Chemistry, Biochemistry and Biophysics, Massey University, Palmerston North, New Zealand.

Abstract

The imposition of magnetic field gradients on a nuclear magnetic resonance experiment imparts a spatial tag to the molecules via the Larmor frequencies of the nuclei (commonly protons) within. A sensitive measure of changes in the frequency distribution is afforded by detecting the loss of phase coherence in a spin-echo experiment performed in the presence of gradient pulses. Here the molecular displacements may be measured over the duration given by the pulse separation. Pulsed field gradient nuclear magnetic resonance (PFGNMR) employs timescales of tens of milliseconds and has a displacement sensitivity of the order 100 nm.

For molecules undergoing Brownian motion, PFGNMR can determine molecular self-diffusion coefficients in liquid and mesomorphic phases down to a lower limit of 10^{-14} m^2 s^{-1}. These coefficients directly probe dynamical processes. For example, in polymer systems such measurements are sensitive to molecular conformation and chain relaxation processes such as reptation. In disperse phases PFGNMR can be used to probe diffusive barriers and reveal molecular organization. The timescale dependence of displacement is especially useful in this regard. Examples of studies on poly- and mono-domain lyotropic liquid crystals are presented.

Recent use of nuclei with spin $>\frac{1}{2}$ offers interesting prospects for PFGNMR. The deuterium quadrupole interaction can be used as a signature for order in anisotropic molecular environments. The preparation in the NMR experiment of tensor polarization, such as states of two quantum coherence, increases precessional dephasing and may yield a considerable increase in displacement sensitivity.

1. Introduction

Molecular translation in the liquid state arises, under conditions of thermodynamic equilibrium, from the Brownian motion due to molecular thermal energy. This self-diffusive motion can only be detected by methods which label individual molecules without introducing thermodynamic gradients, and in this regard nuclear labelling may be regarded as optimally 'non-invasive'.

Three techniques employ such nuclear detection, namely radioactive tracer measurement, neutron scattering spectroscopy and pulsed field gradient nuclear magnetic resonance. Each differs significantly in its sensitivity to molecular displacement. Tracer measurements require macroscopic displacements on the scale of millimetres and are therefore applicable only to molecules undergoing rapid diffusion. At the other extreme, neutron scattering is sensitive to nuclear position correlations over a

* Paper presented at the Australia–New Zealand Condensed Matter Physics Meeting, Pakatoa Island, N.Z., 8–10 February 1984.

0004-9506/84/040359$02.00

few Ångströms and is especially powerful because it directly measures the 'Van Hove correlation function' $P(r_0 \mid r, t)$. This ensemble probability function gives the likelihood of finding a nuclear scattering centre at position and time (r, t) if there was a scattering centre at $(r_0, 0)$. Furthermore, if polarized neutrons are used, separation of the polarized and depolarized scattering cross sections reveals both $P(r_0 \mid r, t)$ and $P_s(r_0 \mid r, t)$ where the latter term is a 'self-correlation' function representing the probability that a scattering centre at r_0 at time zero will have moved to r at a later time t. Neutron scattering is therefore a powerful tool in the study of pair correlations and molecular displacements on the truly microscopic scale.

The subject of this review is pulsed field gradient nuclear magnetic resonance (PFGNMR), a method which is specifically sensitive to the self-correlation function $P_s(r_0 \mid r, t)$, but on a dimensional scale which bridges the gap between neutron scattering and the macroscopic domain. PFGNMR detects molecular self-displacements in excess of a few hundred Ångströms and in consequence lends itself to investigations of structural features in this intermediate regime. We might regard this dimensional scale as the 'organizational domain' of molecules and note that it includes features of macromolecular solutions, mesophase structure of liquid crystals, emulsions and highly disperse biological assemblies. It is the organizational domain applications of the NMR method which is the specific subject of this review, studies which in the solid state would be the proper function of the electron microscope. Nonetheless PFGNMR is an important adjunct in experimental tests of the microscopic theory of simple liquids, especially since it can yield precise self-diffusion coefficients over an exceptionally wide range to a lower limit some three orders of magnitude below that of neutron scattering.

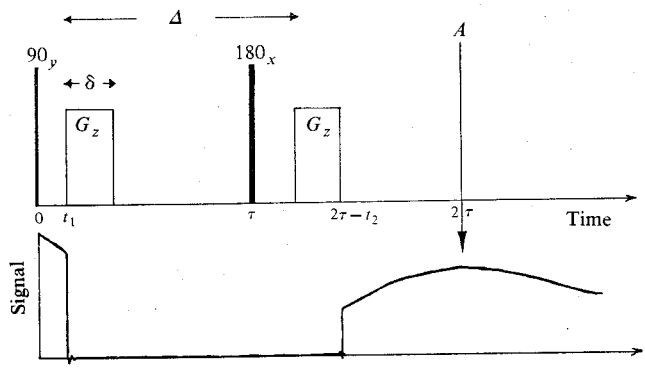

Fig. 1. The r.f. and field gradient pulse sequence showing the experimental times δ, Δ, τ, t_1 and t_2. The vertical arrow indicates where sampling begins.

2. Principles of PFGNMR

Nuclear magnetic resonance provides a molecular label via the characteristic Larmor frequencies of the component nuclei. This label may be given a spatial dependence by the imposition of a well defined magnetic field gradient over the sample space. Very sensitive precessional phase displacements may be detected through the degree of phase refocusing in an NMR spin echo, and the suggestion that these echo signals might be used to measure molecular translational motion was first made by Hahn (1950) when he proposed the spin-echo experiment. A precise theoretical

treatment of this 'constant gradient' NMR experiment was provided by Carr and Purcell (1954).

Because the field gradient spreads the Larmor spectrum, the constant gradient method suffers from the limitation imposed by spectrometer bandwidth. McCall *et al.* (1963) suggested that the gradient might be applied in the form of pulses inserted between the transmit and receive periods of the NMR spin-echo experiment, and this method was later demonstrated and given a detailed theoretical description by Stejskal and Tanner (1965).

The PFGNMR method in its simplest form consists of a two-r.f.-pulse Hahn-echo experiment with identical magnetic field gradient pulses of magnitude G, duration δ and separation Δ applied respectively during the dephasing and rephasing segments of the echo cycle (see Fig. 1). In the limit of intense narrow gradient pulses the experiment is particularly simple to visualize. The first gradient pulse produces a rapid precessional phase shift depending on the position of each nucleus in the sample. Between gradient pulses the molecules containing the nuclei change position, for example because of diffusion. In the intervening period, the 180° r.f. pulse has inverted all prior phase shifts so that the second gradient pulse has the effect of producing phase compensation (or refocusing). To the extent that motion has occurred, the refocusing is incomplete and the consequent attenuation of the spin echo gives a measure of the ensemble average of nuclear translations. The two gradient pulses thus record respectively the initial and subsequent positions of the nuclei over the well defined time scale Δ, and hence PFGNMR is well suited to examining displacement time dependence.

(*a*) *Theory of the Spin-echo Experiment*

In thermal equilibrium the nuclear ensemble is polarized along the static field $B_0\hat{\boldsymbol{k}}$, so that only $\overline{\langle J_z\rangle}$ is nonzero. Components of $\overline{\langle J_x\rangle}$ or $\overline{\langle J_y\rangle}$ are generated by transverse resonant r.f. fields pulsed for a duration sufficient to produce the required flip angle θ. In the laboratory frame such precessing transverse polarization components are detected as an oscillating e.m.f. in the receiver coil. The two-r.f.-pulse spin-echo PFGNMR experiment consists of the sequence $\theta_1|_y$-gradient pulse-$\theta_2|_x$-gradient pulse-echo. We can describe the experiment for general spin angular momentum j by using the density matrix formalism (Abragam 1961). The echo signal amplitude A is the ensemble average expectation value for J_x in the reference frame rotating with the r.f. field, namely,

$$A = \overline{\langle J_x(\text{echo})\rangle} = \text{Tr}\{\rho(\text{echo})J_x\}, \tag{1}$$

where ρ(echo) is the rotating frame density matrix which applies at a time corresponding to the echo centre. If the high temperature and narrow pulse r.f. pulse approximations are employed then

$$\begin{aligned}\rho(\text{echo}) = {} & U^{-1}(\tau')\,R_x^{-1}(\theta_2)\,U^{-1}(\tau)\,R_y^{-1}(\theta_1)\{(\mathscr{I}+\gamma B_0 J_z/k_B T)/(2j+1)\} \\ & \times R_y(\theta_1)\,U(\tau)\,R_x(\theta_2)\,U(\tau'),\end{aligned} \tag{2}$$

where $U(\tau)$ and $U(\tau')$ are respectively the evolution operators before and after the refocusing (θ_2) r.f. pulse, R_x and R_y are rotation operators and γ is the nuclear gyromagnetic ratio. For a Hahn echo θ_1 is 90° and θ_2 is 180°.

For spin-$\frac{1}{2}$ nuclei, such as hydrogen, the Hamiltonian relevant to the evolution operators consists entirely of pseudomagnetic interactions and, in the present instance,

we confine our attention to these. In the rotating frame all secular terms are linear in J_z and the U matrices take the form of z-axis rotation operators, namely

$$U(\tau) = \exp\left(-i\hbar^{-1}\sum \phi J_z\right), \qquad U(\tau') = \exp\left(-i\hbar^{-1}\sum \phi' J_z\right), \qquad (3a,b)$$

where $\Sigma\,\phi$ and $\Sigma\,\phi'$ are variables over the spin ensemble. The effect of the precessions $\Sigma\,\phi$ and $\Sigma\,\phi'$ is to introduce a coefficient $\overline{\exp\{i(\Sigma\,\phi - \Sigma\,\phi')\}}$ into the expression for the transverse magnetization, $\overline{\langle J_x + iJ_y\rangle}$. The phase shifts arise due to precession in the applied magnetic field gradient and due to all other Zeeman terms which 'broaden the resonance line'. For these latter terms the $180|_x$ r.f. pulse causes perfect refocusing and they may henceforth be neglected. In contrast, because of molecular translation, the gradient precession leaves a residual phase displacement ϕ_D for each spin. Spin–spin relaxation provides an additional independent echo attenuation as can be seen by introducing the phenomenological coefficient $\exp(-t/T_2)$ in all off-diagonal elements of the density matrix. Thus the echo amplitude in the presence of the gradient $G(t)$ is

$$\begin{aligned} A(G) &= \mathrm{Tr}\{(J_x + iJ_y)\,\rho(\mathrm{echo})\} \\ &= \overline{\langle J_z(0)\rangle}\exp(-t/T_2)\,\overline{\exp\{i\,\phi_D(\mathrm{echo})\}}, \end{aligned} \qquad (4)$$

so that the analysis of the experiment requires evaluation of the phase displacements ϕ_D and the ensemble average of $\exp\{i\,\phi_D(\mathrm{echo})\}$ taken at the time of the echo maximum. In particular, where the gradient $G(t)$ is given by the pulse sequence of Fig. 1, we define an echo attenuation function

$$R(\boldsymbol{G}, \delta, \Delta) = \overline{\exp\{i\,\phi_D(\mathrm{echo})\}}, \qquad (5)$$

and the dependence of this average on the self-correlation function $P_s(\boldsymbol{r}_0\,|\,\boldsymbol{r}, t)$ may be explicitly described in the special case of narrow gradient pulses, $\delta \ll \Delta$. If, over the period Δ between 'labelling' and 'detection', an individual nucleus displaces by $\boldsymbol{r}-\boldsymbol{r}_0$, then its phase displacement at the time of the echo will be

$$\phi_D = -\gamma\delta(\boldsymbol{r}-\boldsymbol{r}_0)\,.\,\boldsymbol{G}. \qquad (6)$$

Thus, we have

$$R = \iiint_{V_0} P_0(\boldsymbol{r}_0) \iiint_V P_s(\boldsymbol{r}_0\,|\,\boldsymbol{r}, \Delta)\exp\{-i\gamma\delta(\boldsymbol{r}-\boldsymbol{r}_0)\,.\,\boldsymbol{G}\}\,dV\,dV_0, \qquad (7)$$

where $P_0(\boldsymbol{r}_0)$ is the normalized distribution of the initial nuclear spin positions. In equilibrium this distribution is

$$P_0(\boldsymbol{r}_0) = \lim_{t\to\infty} P_s(\boldsymbol{r}_0\,|\,\boldsymbol{r}, t)\,. \qquad (8)$$

The gradient $\boldsymbol{G}$ represents the variation in the polarizing field magnitude along some axis in the sample, so that

$$\boldsymbol{G} = \frac{\partial B_0}{\partial x}\hat{\boldsymbol{i}} + \frac{\partial B_0}{\partial y}\hat{\boldsymbol{j}} + \frac{\partial B_0}{\partial z}\hat{\boldsymbol{k}}. \qquad (9)$$

It is instructive to view equation (7) as a Fourier transformation in which $R(\boldsymbol{G}, \delta, \Delta)$ gives the wavevector spectrum of $P_s(\boldsymbol{r}_0\,|\,\boldsymbol{r}, t)$ appropriately weighted over the nuclear ensemble. To this extent the narrow gradient pulse expression shows that PFGNMR is analogous to a scattering experiment with wavevector $\gamma\delta\boldsymbol{G}$. The frequency spectrum

of $P_s(r_0 \mid r, t)$ may be obtained directly in the time domain by measuring R as a function of Δ.

(b) Description of Molecular Motion

The particular nature of the PFGNMR phase averages represented by equation (5) will depend on the details of the molecular displacements being considered. We might note immediately that where there is no net displacement, which is the case for self-diffusion, $\overline{\exp\{i\phi_D(\text{echo})\}}$ will be real and the echo entirely 'in-phase'. Indeed, the presence of net echo phase shift is the definitive test for directed motion or flow.

Many details of molecular motion under consideration may in principle be revealed by measuring the dependence of the echo attenuation R on the experimental parameters G, δ and Δ. In nearly every case, the use of intense narrow gradient pulses represents an ideal in P_s determination, although in practice finite δ values must be employed to gain sufficient attenuation and in consequence some loss of temporal resolution occurs.

To see how experimental regimes might be categorized it is helpful to begin with the simplest case of isotropic unrestricted self-diffusion. Consider molecules undergoing free Brownian motion with mean square displacements over time t defined by the Einstein relation

$$\overline{(r-r_0)^2} = 6Dt, \tag{10}$$

where D is the molecular self-diffusion coefficient. For such motion, P_s is the solution to the isotropic diffusion equation

$$\partial P_s/\partial t = D\nabla^2 P_s \tag{11}$$

and

$$P_s = (\pi\sigma^2)^{-3/2} \exp\{(r-r_0)^2/\sigma^2\}, \tag{12}$$

where

$$\sigma^2 = 4Dt. \tag{13}$$

Consequently R, the wavevector spectrum of P_s, must also be gaussian and is given by

$$R(\boldsymbol{G}, \delta, \Delta) = \exp(-\gamma^2\delta^2 G^2 D\Delta). \tag{14}$$

Note that since $\overline{(r-r_0)} = 0$, R is real as predicted.

Of course equation (14) is an ideal approximation for $\delta \ll \Delta$. The exact expression for R in the case of unrestricted self-diffusion is well known and is originally due to Stejskal and Tanner (1965) who followed the 'magnetization fluid' approach of Torrey (1956). These authors considered the more general case of a finite steady gradient $\boldsymbol{G}_0$ with superimposed gradient pulses $\boldsymbol{G}$ and showed that

$$\begin{aligned} R = {} & \exp\{-\gamma^2 G^2 D\delta^2(\Delta - \tfrac{1}{3}\delta)\} \exp(-\tfrac{2}{3}G_0^2 D\tau^3) \\ & \times \exp[\gamma^2 \boldsymbol{G}.\boldsymbol{G}_0 D\delta\{t_1^2 + t_2^2 + \delta(t_1+t_2) + \tfrac{2}{3}\delta^2 - 2\tau^2\}]. \end{aligned} \tag{15}$$

The times t_1, t_2 and τ are defined in Fig. 1. The unwanted steady gradient may be considered insignificant when $G_0\tau \ll G\delta$ and in practice this comparison can always be achieved except when studying rapid diffusion of small molecules ($D > 10^{-9}$ $m^2\,s^{-1}$) over echo periods τ in excess of 100 ms. Even in such unfavourable circumstances, the influence of the steady gradient may be suppressed by using, instead of

two r.f. pulses, a closely spaced r.f. pulse train (Meiboom and Gill 1959) in conjunction with the two gradient pulses. Williams *et al.* (1978) have shown that the effect of the gradient pulses in this experiment is equivalent to that which applies in the simple Hahn-echo sequence. In practice therefore, the Stejskal–Tanner equation reduces to

$$R = \exp\{-\gamma^2 G^2 D\delta^2(\Delta - \tfrac{1}{3}\delta)\}. \tag{16}$$

Comparison with equation (14) suggests that the narrow pulse evaluation of R is substantially correct but, for finite δ, the effective diffusive observation time takes the reduced value

$$\Delta_r = \Delta - \tfrac{1}{3}\delta. \tag{17}$$

In fact this evaluation is only exactly true when P_s is gaussian. This is apparent when one considers the phase distribution approach of Carr and Purcell (1954) from which the Stejskal–Tanner equation can be independently derived (Williams *et al.* 1978). In this model it is allowed that, even where P_s is non-gaussian, evolution of random phase displacements due to diffusion during the finite gradient will cause the phase distribution $P(\phi_D)$ to be gaussian as a consequence of the central-limits theorem. Thus, only in the narrow pulse limit is the spatial spectrum of P_s directly revealed. The use of finite gradient pulses will always tend to degrade the dependence of R on G to a gaussian. Nonetheless the use of equation (7) for more complex P_s functions with Δ replaced by the reduced time Δ_r is a valid first approximation where δ is finite. Indeed, the usefulness of this approximation is indicated by the fact that an exact analytic expression for R under finite δ has only ever been obtained for the case of unbounded self-diffusion!

An experimental approach to more complex motion might be as follows. Consider a narrow pulse experiment on a single molecular species in which the echo attenuation is real but the dependence of $\ln R$ on G^2 is nonlinear. Despite the fact that the net displacements are apparently zero we may say that the motion is not isotropic Brownian. In the case that the motion consists of inhomogenous or anisotropic self-diffusion, R will be a superposition of gaussians having a common exponential parameter $G^2\delta^2\Delta_r$. Such a gaussian superposition can be demonstrated by varying G and Δ independently and observing such a common echo dependence in which R is uniquely determined by the value of $G^2\delta^2\Delta_r$. Now let us suppose that plots of $\ln R$ against $G^2\delta^2\Delta_r$ do not superpose as Δ is varied. We may then conclude that the distance moved by the molecules in the time Δ is comparable with the spacing of some boundaries offering restriction to the motion. We use the term restricted diffusion to classify such experiments. In the extreme case that R is entirely independent of Δ we may say that the molecules are totally confined and, in the experimental timescale, P_s assumes its asymptotic value P_0.

The Δ dependence of the echo attenuation is the crucial experimental test for the presence and dimension of diffusive barriers and will be applied to examples discussed below.

(*c*) *Experimental Considerations*

Details of the apparatus required for spin-echo NMR and pulsed field gradient generation are given elsewhere (Callaghan *et al.* 1980*b*; Fukushima and Roeder 1981). Special problems do arise in the form of echo instability and distortion unless appropriate precautions are taken. Residual steady gradients should be minimized and can

typically be reduced to $<0{\cdot}1\ \mathrm{mT\,m^{-1}}$ in comparison with gradient pulse strengths which can easily be produced in excess of $1{\cdot}0\ \mathrm{T\,m^{-1}}$.

Magnetic field gradients may be produced using either opposed Helmholtz (Tanner 1965) or quadrupolar coils (Webster and Marsden 1974), the latter being superior in the convenience of their geometry, their smaller inductance/gradient ratio and the ease with which orthogonal independent $\partial B_0/\partial x$ and $\partial B_0/\partial z$ gradients may be incorporated in the one assembly.

Protons offer the greatest sensitivity in NMR because of their high gyromagnetic ratio, although PFGNMR experiments have been reported using ^{13}C, ^{2}H, ^{19}F and ^{7}Li (Lindman *et al.* 1981; Murday and Cotts 1970; Callaghan *et al.* 1983*b*; Gordon and Strange 1978; Murday and Cotts 1968). In most circumstances, however, ^{1}H where available is the preferred molecular label. It is noted that the ultimate limitation to spin-echo signal-to-noise is the nuclear relaxation time T_2. Irreversible decay of the magnetization, due to spin–spin relaxation, limits the time Δ over which PFGNMR measurements are possible and, in practice, confines the observation to molecules whose nuclei have, on a local molecular scale, a 'liquid-like' isotropic reorientational behaviour. Problems associated with short T_2 can be circumvented in a few special circumstances, notably where the spin lattice relaxation time T_1 greatly exceeds T_2. Here the stimulated echo method can prove useful (Tanner 1970). For practical purposes, in particular because of the size of available gradients, we require T_2 greater than a few milliseconds since gradient pulse spacings are required to occupy the millisecond regime if significant attenuations are to be obtained on systems of interest. PFGNMR therefore probes the temporal spectrum of P_s at frequencies below 1 kHz and the spatial spectrum at wavenumbers below $10^5\ \mathrm{cm^{-1}}$.

3. Isotropic Self-diffusion

(*a*) *Self-diffusion in Simple Liquids*

Experimental tests of the Stejskal–Tanner relation (16) for molecules undergoing unhindered isotropic Brownian motion show it to be precisely obeyed as evident in Fig. 2 (Callaghan *et al.* 1983*b*). These plots display echo attenuation data plotted as $\ln R$ versus $I^2\delta^2\Delta_r$ (where I is the gradient coil current) for proton and deuteron observation in H_2O and D_2O respectively. Such experiments may be used to calibrate the gradient coil and indeed the most precisely known self-diffusion coefficients suitable for such a purpose are those obtained for normal and heavy water by Mills (1973) using radioactive tracer methods. The data of Fig. 2 independently yield the same coil calibration factor within experimental error. Furthermore, a PFGNMR experiment using independent proton and deuteron observation on a single molecular species, d1-benzene, gives the same self-diffusion coefficient. Equation (16) has therefore been tested for its dependence on G, δ, γ and Δ and found to be entirely accurate within the available experimental precision of $\pm 1\%$.

NMR permits molecular resolution because of differences in nuclear Larmor frequencies arising from specific labelling with a differing nuclear species or, in the case that the observed nucleus is common, by means of the chemical shift. PFGNMR thus offers a method of determining independent self-diffusion coefficients of components in simple liquid mixtures (James and Macdonald 1973). Fig. 3 illustrates the alternative labelling methods. In Fig. 3*a* (Callaghan *et al.* 1983*b*),

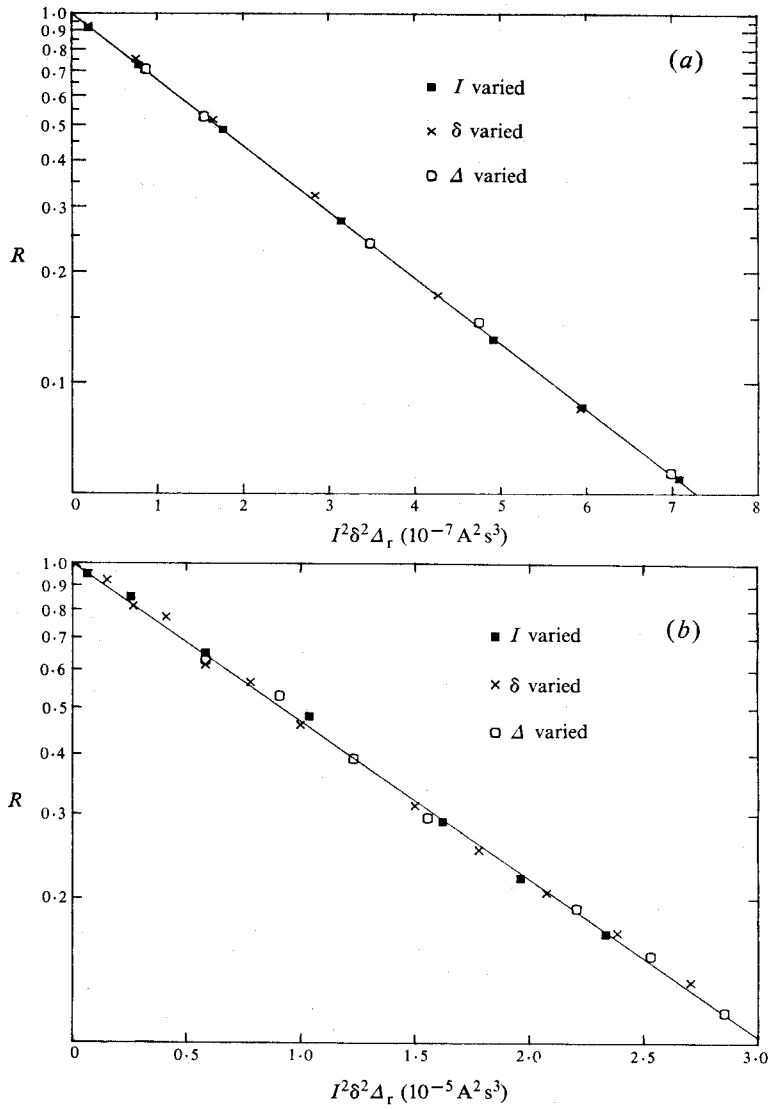

Fig. 2. Echo attenuation plots for (*a*) ^{1}H nuclei in H_2O and (*b*) ^{2}H nuclei in D_2O at 25°C. The gradient coil current I, pulse width δ, and pulse separation Δ are all varied.

the dependence of the diffusion of proton and deuteron containing species (H_2O, HDO) and (HDO, D_2O) is shown for normal/heavy water mixtures. In Fig. 3*b* (Callaghan *et al.* 1980*b*) the proton signals from benzene and butanol are resolved to reveal the independent self-diffusion coefficients in a 50 : 50 mixture.

(*b*) *Macromolecules*

High polymer molecules in solution are the subject of interest both in their conformation and in their intra- and inter-molecular dynamical processes. In biological examples, a knowledge of the shape of a macromolecule in solution may reveal aspects

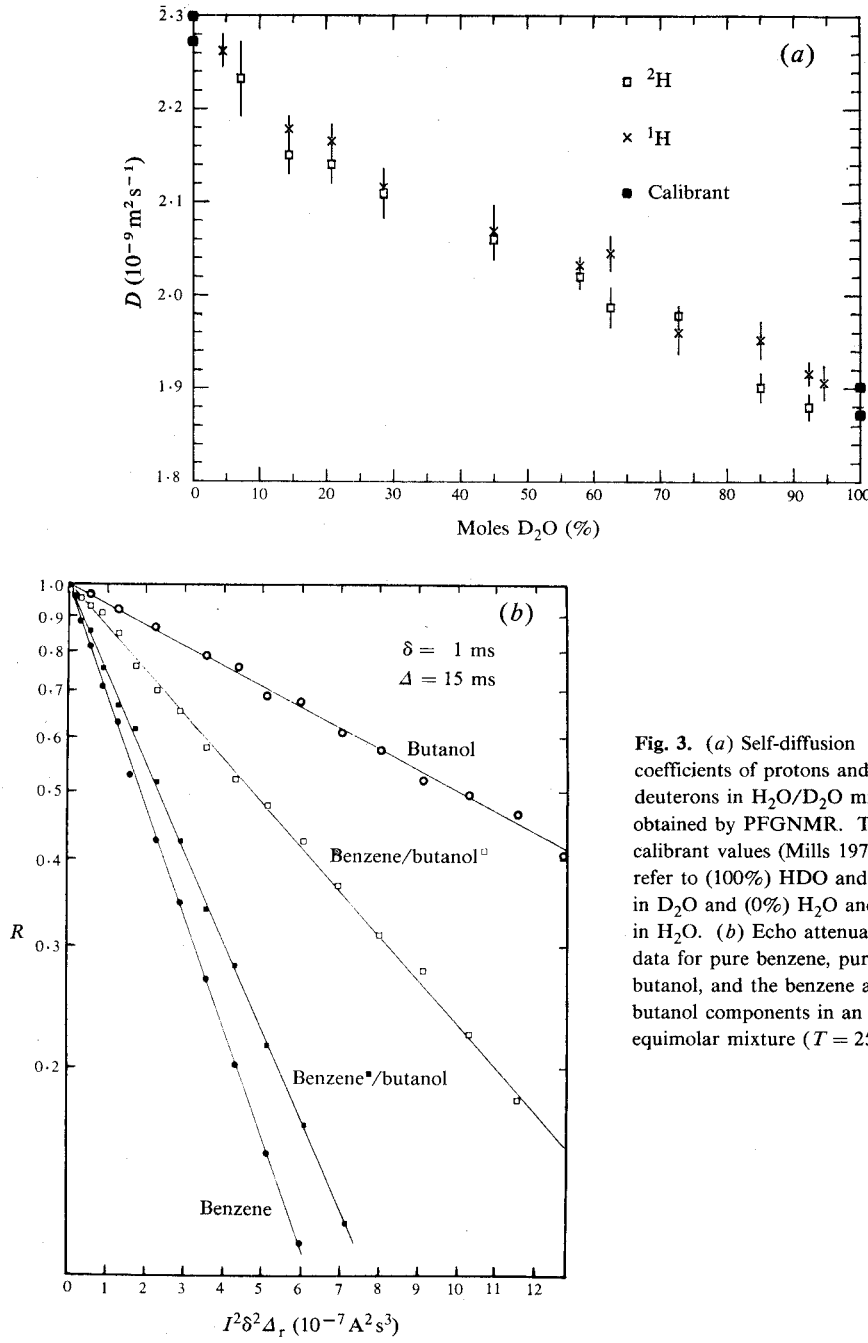

Fig. 3. (*a*) Self-diffusion coefficients of protons and deuterons in H_2O/D_2O mixtures obtained by PFGNMR. The calibrant values (Mills 1973) refer to (100%) HDO and D_2O in D_2O and (0%) H_2O and HDO in H_2O. (*b*) Echo attenuation data for pure benzene, pure butanol, and the benzene and butanol components in an equimolar mixture ($T = 25°C$).

of its biological function. In contrast, studies of ideal random flight polymers provide a test of renormalization group models relevant to critical phenomena.

We consider first the biological problem: what is the shape of a highly branched polysaccharide or globular protein in solution? In such solutions the effective solvent diffusion is reduced because the solvent molecules are obliged to divert tortuously

around obstructions presented by the macromolecules. In addition to this 'obstruction' effect, the average diffusion coefficient will be further attenuated if the solvent molecules spend some of their time associated with the much more slowly moving macromolecules. This might be termed a 'solvation' effect. Both the obstruction and solvation effects have been incorporated by Wang (1954) in a model in which the solvent self-diffusion coefficient D^{solv} is related to a macromolecular shape factor $\bar{\alpha}$. The expression for diffusive reduction is (Clark *et al.* 1982)

$$D^{solv} = D_0^{solv}[1 - w\{(\bar{\alpha}-1)(\bar{V}_p d_0 + h) + h\}], \tag{18}$$

where w is the macromolecular weight fraction, $\bar{V}_p$ the apparent macromolecular specific volume, d_0 the density of the pure solvent and h the solvation coefficient (gram per solvent/gram per solute). Further, D_0^{solv} is the pure solvent self-diffusion coefficient and $\bar{\alpha}$ can be defined in terms of the ellipsoidal parameter ρ, the ratio of the major to minor axis. For an oblate ellipsoid we have

$$\bar{\alpha} = \tfrac{1}{3}\left(1 - \frac{\rho}{1-\rho^2}\left((1-\rho^2)^{-\frac{1}{2}}[\tan^{-1}\{\rho/(1-\rho^2)^{\frac{1}{2}}\} - \tfrac{1}{2}\pi] + \rho^{-1}\right)\right)^{-1}$$
$$+ \tfrac{4}{3}\left(\frac{2-\rho^2}{1-\rho^2} - \frac{\rho}{(1-\rho^2)^{3/2}}[\tfrac{1}{2}\pi - \tan^{-1}\{\rho/(1-\rho^2)^{\frac{1}{2}}\}]\right)^{-1}. \tag{19}$$

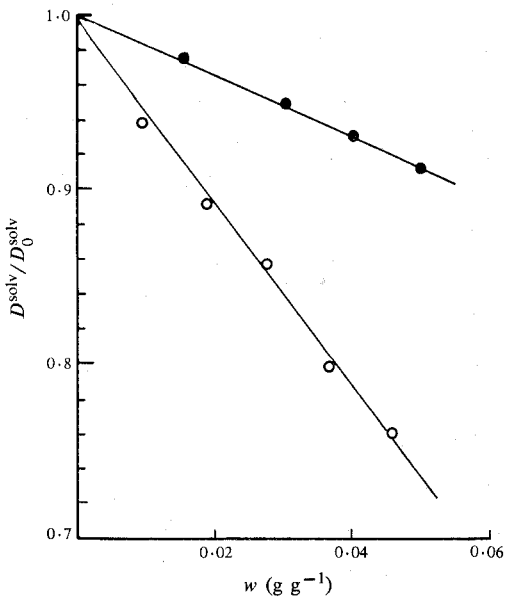

Fig. 4. Dependence of solvent diffusion on amylopectin concentration w for wheat starch amylopectin in dimethylsulfoxide (open circles) and D_2O (closed circles). The data are fitted to yield shape factors $\bar{\alpha}$.

Derbyshire and Duff (1973) have used PFGNMR to deduce $\bar{\alpha}$ for agarose gel. These authors showed further that h can be obtained using NMR by measuring the fraction of solvent molecules which remain in the liquid state on reducing the sample temperature below the solvent freezing point. Shape factors have similarly been obtained for ovalbumin and bovine–serumalbumin (Clark *et al.* 1982). Fig. 4 shows diffusive attenuation data for wheat starch amylopectin in two solvents, water and dimethylsulfoxide (Callaghan and Lelievre 1984). The macromolecule is highly planar in the organic solvent but exhibits a more spherical shape as a result of aggregation in water.

While solvent self-diffusion can indirectly reveal some features of macromolecular shape, the self-diffusion coefficients of the macromolecules themselves contain inherently more information. Consider for example the case of infinite dilution, for which the self-diffusion coefficient D_0 can be written in terms of the Stokes–Einstein expression

$$D_0 = k_B T/6\pi\eta R_D, \tag{20}$$

where η is the solvent viscosity and R_D is the molecular hydrodynamic radius which may therefore be directly obtained by D_0 measurement. As the concentration is increased, the effective friction $6\pi\eta R_D$ will increase in a manner which depends on molecular shape and molar volume v_M. This dependence appears in a virial expansion:

$$D^{-1} = D_0^{-1}(1 + k_f c + \ldots). \tag{21}$$

Yamakawa (1968) expressed k_f for a polymer of molecular mass M in terms of the second virial coefficient A_2:

$$k_f = 1 \cdot 2A_2 M + N_A v_M M^{-1}. \tag{22}$$

For an oblate ellipsoid (non-free-draining) Yamakawa (1971) gave

$$A_2 = 4N_A v_M M^{-2} f_c, \tag{23}$$

where

$$f_c = \tfrac{1}{4} + \tfrac{3}{16}[1 + \rho\{\sin(1-\rho^{-2})^{\frac{1}{2}}\}/(1-\rho^{-2})^{\frac{1}{2}}] \times \left(1 + \{\rho^{-2}/2(1-\rho^{-2})^{\frac{1}{2}}\} \ln[\{\rho + (\rho^2-1)^{\frac{1}{2}}\}/\{\rho - (\rho^2-1)^{\frac{1}{2}}\}]\right). \tag{24}$$

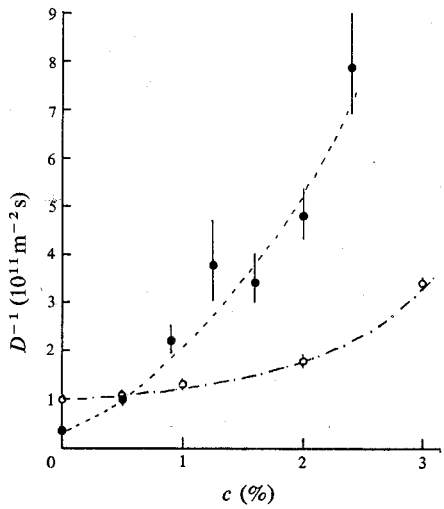

Fig. 5. Concentration dependence for self-diffusion of dilute amylopectin in D_2O (open circles) and dimethylsulfoxide (closed circles) at 24°C. The data yield relative molecular sizes and shapes in the two solvents.

Fig. 5 shows the result of a high dilution PFGNMR study of amylopectin self-diffusion in water and dimethylsulfoxide. The different D_0 values indicate the relative molecular sizes, again suggesting aggregation in water, while the initial slopes of D_0 versus concentration c indicate the comparative axial ratios.

The study of synthetic random coil macromolecules in solution is well suited to PFGNMR since the high monomer rotational mobility in polymers such as polystyrene leads to long spin–spin relaxation times. In Fig. 6 (Callaghan and Pinder 1981)

the variation of D_0 with molecular mass for polystyrene in carbon tetrachloride lends support to the Flory (1971) scaling relation

$$R_D = M^{\nu}, \tag{25}$$

where ν is a critical exponent which varies between the asymptotes $\frac{1}{2}$ and $\frac{3}{5}$ depending on solvent–monomer interactions (Weill and des Cloizeaux 1979).

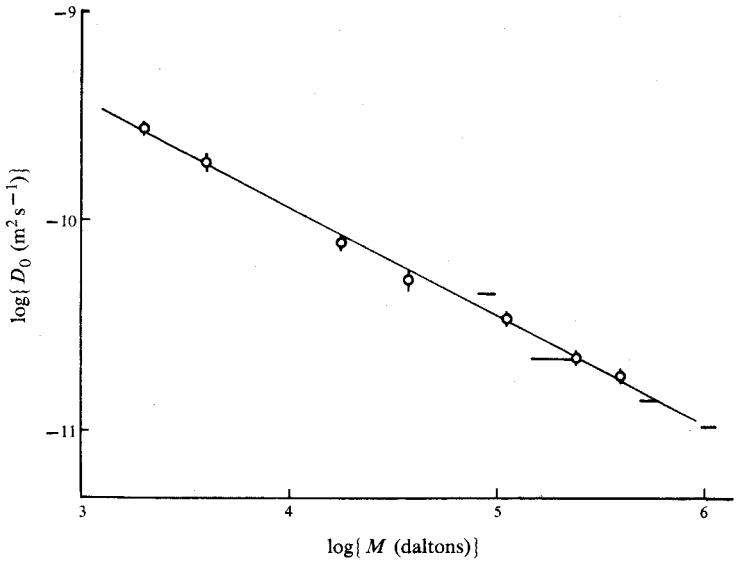

Fig. 6. Log plot of the self-diffusion coefficient D_0 against the molecular mass M for polystyrene in carbon tetrachloride (open circles) at 28°C (Callaghan and Pinder 1981). The data scale as $D_0 \sim M^{0.51(2)}$. Bar data are from mutual diffusion methods (Schick and Singer 1950).

At concentrations sufficient for coil overlap, the solution is termed semi-dilute with the boundary concentration between dilute and semi-dilute regimes accorded the symbol c^*, where

$$c^* = MR^{-3} \tag{26}$$

and R is the molecular static radius. The onset of coil overlap and entanglement is signalled by a steep inverse concentration dependence of self-diffusion. According to the reptation theory of de Gennes (1976), semi-dilute random coils undergo a curvilinear diffusion in a tube of diameter ξ, which is the mean distance between topological constraints to the free motion of the chain. This distance ξ is a governing length scale for physical processes in the semi-dilute regime, and the reptation time T_r, for the coil to diffuse its length along the tube, is a characteristic relaxation time. Measurement of semi-dilute polymer D values provides an important test of the reptation theory. This theory predicts that

$$D \sim M^{-2}c^{(2-\nu)/(1-3\nu)}, \tag{27}$$

which in the good solvent limit, $\nu = \frac{3}{5}$, gives

$$D \sim M^{-2}c^{-1.75}. \tag{28}$$

The data of Fig. 7 for polystyrene in carbon tetrachloride (Callaghan and Pinder 1984) illustrate that the concentration dependence obeys the $c^{-1.75}$ scaling law only as an asymptotic behaviour at low concentrations in the semi-dilute regime. This observation is consistent with the crossover model of Pouyet *et al.* (1980) and Callaghan and Pinder (1981). These authors proposed that the chain statistics vary between gaussian ($D \sim c^{-3}$) and excluded volume ($D \sim c^{-1.75}$) as the size of the length scale

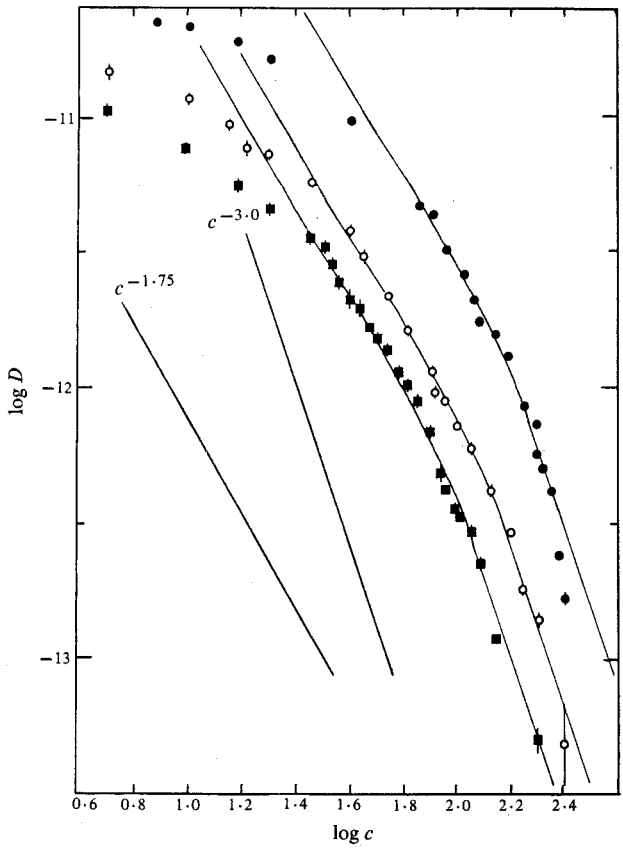

Fig. 7. Self-diffusion of polystyrene in carbon tetrachloride at 28·0°C for molecular masses of 110 000 (closed circles), 233 000 (open circles) and 350 000 (squares) daltons near the semi-dilute regime. The curves are the theoretical predictions of the crossover model (Weill and des Cloizeaux 1979) applied to the de Gennes (1976) reptational model. Simple reptational scaling is only apparent in the asymptotic high and low concentration regimes.

ξ is varied with changes in concentration. Furthermore the data of Fig. 7 reveal that crossover effects are molecular mass dependent and this fact undermines the simple scaling law $D \sim M^{-2}$. The PFGNMR measurements of polymer self-diffusion are more precise than those attainable by other methods and, in the instance cited, have placed the reptation model under close scrutiny.

4. Anisotropic Diffusion

We now turn our attention to PFGNMR measurements in systems where the diffusion displays an obvious anisotropy. In general the self-correlation function obeys a self-diffusion equation of the form

$$\partial P_s/\partial t = \nabla . \mathbf{D} \nabla P_s , \tag{29}$$

where the self-diffusion coefficient is a cartesian tensor. It is then necessary to replace $G^2 D$ by $\boldsymbol{G} . \mathbf{D} . \boldsymbol{G}$ in expressions for the PFGNMR echo attenuation. For structures of right symmetry, $\mathbf{D}$ is diagonal. For example, in nematic and smectic A liquid crystals one finds $D_{z'z'} = D'_{\|}$ and $D_{x'x'} = D_{y'y'} = D'_{\perp}$, the primed axes referring to the coordinates of the molecular director. In the unprimed laboratory coordinates, oriented with respect to the director by colatitude Θ and azimuth Φ, one obtains

$$\mathbf{D} = R^{-1}(\Theta, \Phi) \mathbf{D}' R(\Theta, \Phi) , \tag{30}$$

with $R(\Theta, \Phi)$ a coordinate rotation matrix. The dependence of $\mathbf{D}$ on director orientation provides an important structural test. As a simple example, the sense of the anisotropy, $D_{\perp}/D_{\|}$, is opposite in nematic and smectic phases.

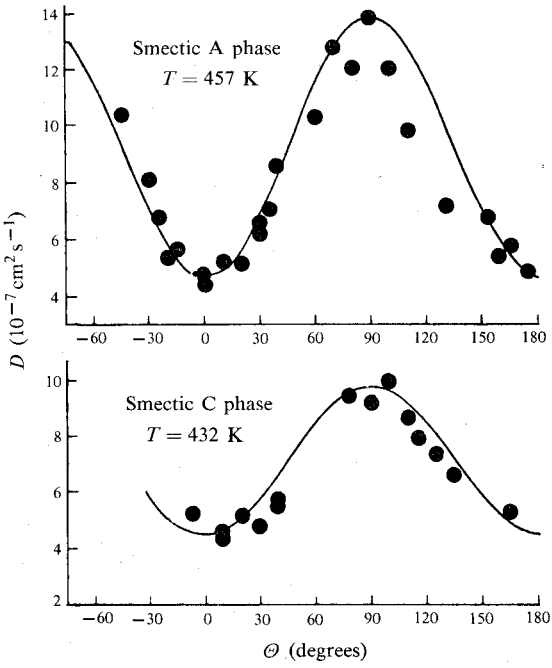

Fig. 8. Angular dependence of the self-diffusion coefficient of TBBA in the smectic A and smectic C phases from Blinc *et al.* (1974). The angle between the field gradient and the molecular directors is Θ. The theoretical fits give a measure of diffusion anisotropy.

PFGNMR has been used to investigate diffusion in nematic liquid crystals (Hayter *et al.* 1974; Zupancic *et al.* 1974). In a study of the water diffusion in nematic perfluorooctanoate/water mesophases, the low diffusion anisotropy has been related to the shape of nematic aggregates (Boden *et al.* 1984). Blinc *et al.* (1974) have obtained the angular dependence of TBBA self-diffusion, shown in Fig. 8, for oriented smectic A and smectic C phases. The attenuation of the diffusion anisotropy in the smectic C case is attributable to director tilt with respect to the smectic layers and the self-diffusion measurements help to characterize the orientational order in this phase.

In amphiphilic lyotropic liquid crystals such as soap/water systems, solvent molecules in the lamellar phase exhibit a high diffusion anisotropy. Fig. 9 shows a PFGNMR measurement of $D_\perp$ and $D_\parallel$ for heavy water between potassium palmitate bilayers, oriented by interleaving the liquid crystal between the sheets of a glass stack (Callaghan *et al.* 1983*b*). These authors found $D_\perp/D_\parallel = 30$, in agreement with earlier measurements by proton PFGNMR. The thickness of the water layer ($\sim$100 Å) is too small to enable observation of single layer displacements normal to the lamellae (i.e. in the $\parallel$ direction), and the PFGNMR measurement of $D_\parallel$ is sensitive to displacements over many bilayers. The measured $D_\parallel$ is in fact determined by the trans-bilayer permeation rate.

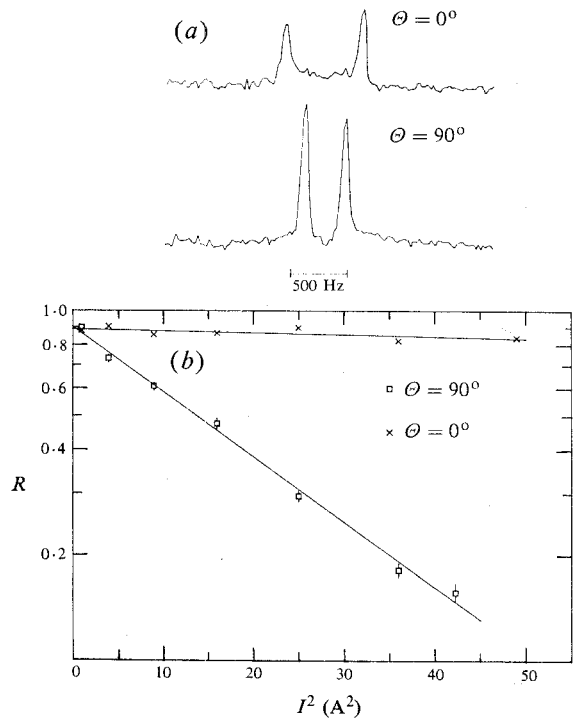

Fig. 9. (*a*) Deuterium NMR solid-echo spectra for oriented single crystalline potassium palmitate/D_2O bilayers (50 : 50 w/w) at 65°C (2τ = 24 ms). The splittings for orientation at 0° and 90° to the external field are in the predicted lamellar phase ratio of 2 : 1. (*b*) Deuterium PFGNMR solid-echo attenuation for the sample in (*a*), illustrating anisotropic water diffusion (Δ = 12 ms and δ = 8 ms).

Most amphiphilic liquid crystals form a poly-domain structure unless special methods as described above are used to orient them. The laboratory frame description of the PFGNMR experiment in these systems is therefore complicated by the need to perform a 'powder average'. The analysis is, however, considerably simplified if the diffusing molecules remain in a single domain, of unique local director orientation, over the timescale of the experiment. That such residence can occur is illustrated in

Fig. 10 where the quadrupole interaction for D_2O in polycrystalline potassium palmitate/water gives a splitting dependent on the local director orientation with respect to the magnetic field (Callaghan *et al.* 1983*b*). Under the PFGNMR experiment the water in the lamellae with directors at 90° to the field gradient exhibit enhanced attenuation. Quantitative analysis of different parts of the spectrum is consistent with water molecules having the predicted and constant local component of diffusion along the external field direction.

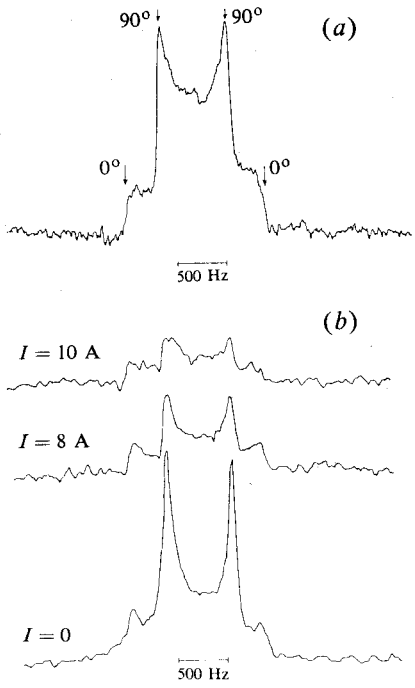

Fig. 10. Deuterium NMR solid-echo spectra for polycrystalline potassium palmitate/D_2O (70:30 w/w) at 65°C for (*a*) $2\tau = 4$ ms and (*b*) $2\tau = 24$ ms. In (*b*) the spectrum is shown as a function of field gradient pulse strength and there exists a clear correspondence within the spectrum between the director orientations and the components of diffusion along the field gradient.

For ordered liquids exhibiting axial symmetry, such as is the case for the water layers in amphiphilic lamellar mesophases, the azimuthal dependence in equation (30) disappears and we may write

$$\overline{z^2} = 2D_{\parallel}\Delta_r \cos^2\Theta + 2D_{\perp}\Delta_r \sin^2\Theta, \tag{31}$$

where $\overline{z^2}$ is the mean square displacement along the field gradient axis in the reduced time Δ_r. Hence R is obtained by averaging element orientations over all angles and, writing $k = \gamma^2 G^2 \delta^2 \Delta_r$, we have

$$R = \int_0^{\pi} \exp\{-k(D_{\parallel}\cos^2\Theta + D_{\perp}\sin^2\Theta)\}\sin\Theta \, d\Theta \Big/ \int_0^{\pi} \sin\Theta \, d\Theta, \tag{32}$$

and thus

$$R = \exp(-kD_{\perp}) \int_0^1 \exp\{-k(D_{\parallel} - D_{\perp})x^2\} \, dx. \tag{33}$$

For high anisotropy of the type $D_{\perp} \gg D_{\parallel}$ we then obtain so-called two-dimensional behaviour:

$$R_2 = \exp(-kD_{\perp}) \int_0^1 \exp(kD_{\perp}x^2) \, dx. \tag{34}$$

The echo dependence represented by equation (34) may be used as a signature for poly-domain lamellar diffusion anisotropy. In Fig. 11 the echo attenuation plot obtained for water protons in Aerosol OT/water exhibits such behaviour and indicates poly-domain lamellar structure (Callaghan and Soderman 1983). Note that as Δ is varied the data display a common dependence on $G^2\delta^2\Delta_r$, indicative of a gaussian superposition of components undergoing Brownian motion along the field gradient axis each with a fixed diffusion coefficient. This observation confirms that the curvature in the plot of $\ln R$ versus G^2 arises from anisotropic and not restricted diffusion. In fact as Δ is increased sufficiently for molecules to sample different local director orientations, this behaviour breaks down.

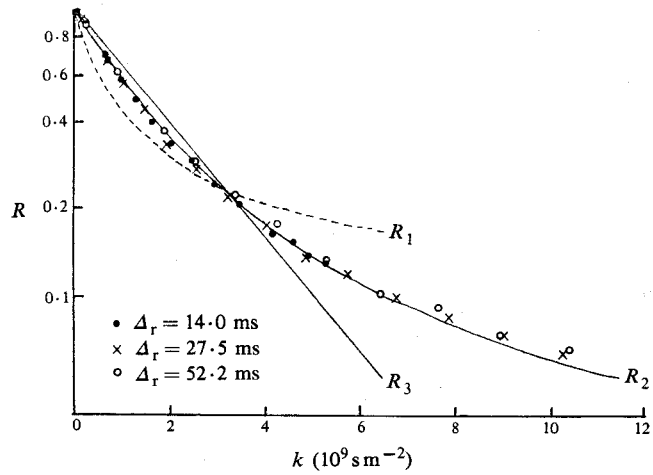

Fig. 11. Dependence of water proton echo attenuation for 24·8% Aerosol OT/water on the parameter $k = \gamma^2G^2\delta^2\Delta_r$. The theoretical curves labelled R_1, R_2 and R_3 refer to one-, two- and three-dimensional diffusion [equations (35), (34) and (16) respectively]. The reduced observation time is varied between 14·0 and 52·2 ms and the data lie on a common curve characteristic of two-dimensional diffusion. This indicates that, for these observation times, each water molecule in the poly-domain sample resides locally in lamellae belonging to a single domain.

The usefulness of PFGNMR in helping to characterize liquid crystalline phases is shown in Fig. 12, again for lamellar Aerosol OT. The water self-diffusion displays a significant increase exactly in the concentration region where X-ray diffraction suggests anomalous halving of bilayer spacing, despite the fact that swelling experiments show normal behaviour right across the lamellar phase. Furthermore, a transition to isotropic three-dimensional diffusion correlates with a region of high electrical conductivity, tending to confirm the suggestion that domain walls are in motion. The hypothesis consistent with the Aerosol OT lamellar phase anomalies concerns the formation of amphiphile 'bridges' across the water layer, as shown in Fig. 13. These bridges break to form a disc of interleaved bilayers when the water layer thickness is reduced below 50 Å.

In some systems a strong opposite anisotropy of the sense $D_\perp \ll D_\parallel$ will apply. Such behaviour may be termed 'capillary'. Here we expect

$$R_1 = \int_0^1 \exp(-kD_\parallel x^2)\,dx \qquad (35)$$

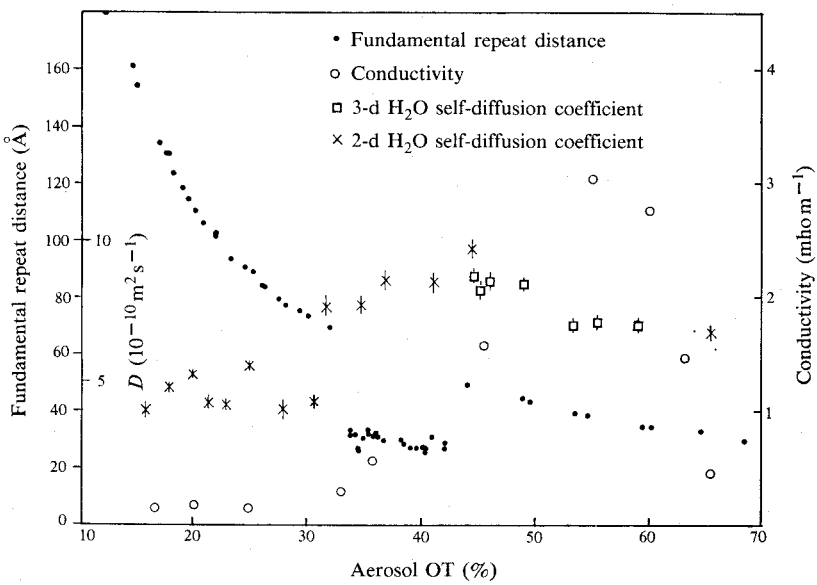

Fig. 12. Superposition of X-ray, conductivity and self-diffusion behaviour for the lamellar phase of Aerosol OT/water as the amphiphile concentration is varied. A correspondence in behavioural regimes is apparent. Self-diffusion coefficients are obtained by either R_2 or R_3 fits as appropriate.

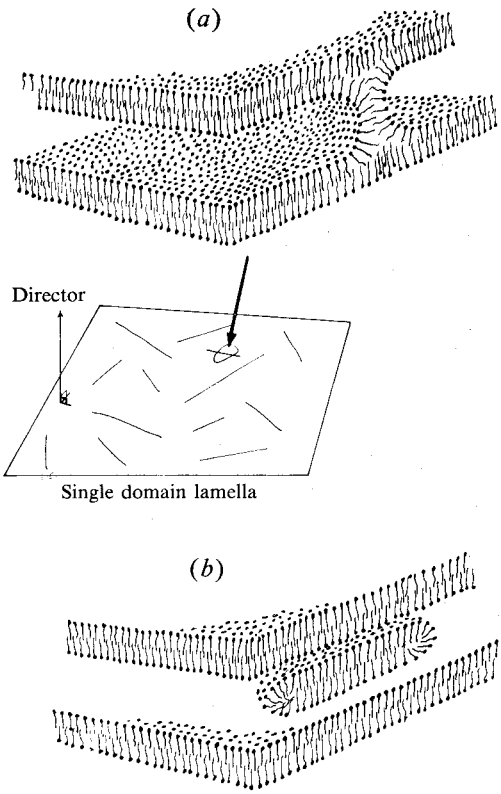

Fig. 13. Proposed amphiphile organization for (*a*) low concentration and (*b*) intermediate concentration regimes in Aerosol OT/water. In (*a*) regions of admixed reversed hexagonal phase constitute barriers to diffusion.

and, in Fig. 14, we see the consistency of this model with the measured proton echo attenuation from water in wheat grain endosperm tissue (Callaghan *et al.* 1979). It is concluded that the adsorbed moisture is trapped on the surface of extended protein fibres.

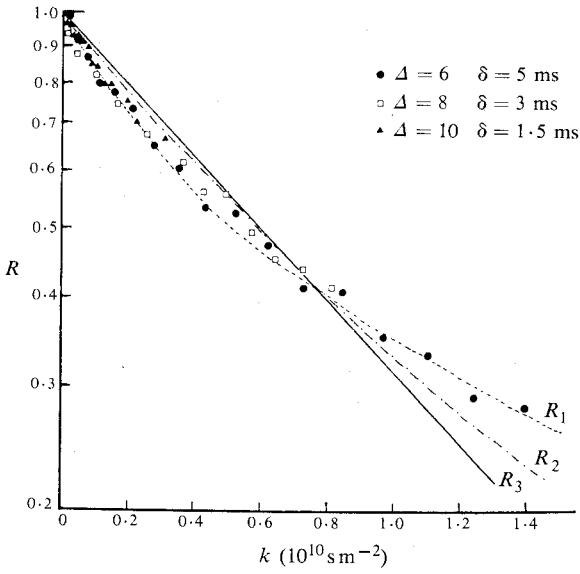

Fig. 14. Echo attenuation versus k for water in wheat grain endosperm tissue equilibrated to 90% R.H. at 22°C. Once again the common dependence on k indicates free Brownian motion within local single domains but here the theoretical fit indicates that the water is confined to capillary motion in one dimension.

5. Restricted Diffusion

Where molecules encounter some boundary modifying their diffusive motion, the distribution of displacements no longer engenders $P_s(\boldsymbol{r}_0 \mid \boldsymbol{r}, t)$ with a time dependence characteristic of Brownian motion. In the event that the displacements are large enough to be detected by PFGNMR, such deviant behaviour will be manifested as a deviation of the echo attenuation from dependence on $G^2\delta^2\Delta_r$ alone. In the narrow pulse approximation, PFGNMR can in principle yield the entire spatial and temporal properties of P_s. In practice there are limitations (e.g. T_2) to the spectrum of P_s which can be sampled and experiments are generally less ambitious, where some proposed P_s function is tested by predicting and comparing with data the echo attenuation over the experimentally available range of G and Δ.

Theoretical echo attenuations based on equation (7) have been calculated for a variety of fundamental geometries as follows.

(*a*) *Laminar Boundaries*

In the examples dealing with anisotropic diffusion in liquid crystals it was noted that for two-dimensional behaviour in amphiphilic lamellar phases, the displacements perpendicular to the obstructing amphiphile surfaces were insufficient to be detected and in consequence $D_{\|}$ could be assigned a zero value. Suppose instead that the interlamellar layer spacing a is sufficiently large (e.g. of order μm) that such displacements are detectable. It is then appropriate to regard interlamellar molecules as diffusing isotropically but with unbounded freedom only along the two dimensions parallel to the laminar barrier. For this case it has been shown by Tanner and Stejskal (1968) that

$$P_s(r_0 \mid r, t) = (4\pi a D t)^{-1} \exp\{-(r-r_0)_\perp^2/4Dt\}$$
$$\times\left\{1 + 2\sum_{n=1}^{\infty} \exp\left(\frac{-n^2\pi^2 Dt}{a^2}\right) \cos\left(\frac{n\pi r_\parallel}{a}\right) \cos\left(\frac{n\pi r_{0\parallel}}{a}\right)\right\}, \quad (36)$$

with $P_0(r_0)$ constant everywhere inside the layer. Hence we have

$$R = \exp(-\gamma^2 G_\perp^2 \delta^2 \Delta D)\left\{\frac{2\{1-\cos(\gamma\delta G_\parallel a)\}}{(\gamma\delta G_\parallel a)^2}\right.$$
$$\left. + 4(\gamma\delta G_\parallel a)^2 \sum_{n=1}^{\infty} \exp\left(\frac{-n^2\pi^2 D\Delta}{a^2}\right) \frac{1-(-1)^n \cos(\gamma\delta G_\parallel a)}{\{(\gamma\delta G_\parallel a)^2 - (n\pi)^2\}^2}\right\}. \quad (37)$$

This dependence of R on observation time Δ has been partially demonstrated by Tanner and Stejskal (1968) for water diffusing perpendicular to the leaves of a mica stack. The asymptotic behaviour of R is of interest where the field gradient is oriented normally to the obstructing layers ($G_\perp = 0$, $G_\parallel = G$):

$$R_\infty = \lim_{\Delta\to\infty} R = 2\{1-\cos(\gamma\delta G a)\}/(\gamma\delta G a)^2. \quad (38)$$

This independence of R from Δ is characteristic of particles trapped in the direction of the applied gradient.

If the obstructing layer has finite permeability p, Tanner (1978) has shown that $\ln R$ approaches an asymptote once again linear in $G^2\delta^2\Delta_r$, thus implying an effective diffusion coefficient normal to the barriers of

$$\lim_{\Delta\to\infty} D = (1+p^{-1})^{-1} \lim_{\Delta\to 0} D. \quad (39)$$

(*b*) *Spherical Boundaries*

An entirely similar approach applies for particles diffusing in a spherical cavity, although the mathematical complexity is somewhat increased. Under an assumption of gaussian phase displacements, Murday and Cotts (1968) derived for the case of an impermeable spherical cavity of radius R_0

$$R = \exp\left(-2\gamma^2 G^2 \sum_{m=1}^{\infty} f(\alpha_m)\right), \quad (40)$$

with

$$f(\alpha_m) = \{\alpha_m^2(\alpha_m^2 R_0^2 - 2)\}^{-1}$$
$$\times\left\{\frac{2\delta}{\alpha_m^2 D} - \left(\frac{2+\exp\{-\alpha_m^2 D(\tau-\delta)\} - 2\exp(-\alpha_m^2 D\delta)}{(\alpha_m^2 D)^2}\right.\right.$$
$$\left.\left. - \frac{2\exp(\alpha_m^2 D\tau) + \exp\{-\alpha_m^2 D(\tau+\delta)\}}{(\alpha_m^2 D)^2}\right)\right\}. \quad (41)$$

The α_m are roots of the equation

$$\alpha_m R_0 J'_{3/2}(\alpha_m R_0) - \tfrac{1}{2} J_{3/2}(\alpha_m R_0) = 0. \quad (42)$$

In the asymptotic limit, $D\tau \gg R_0^2$, the expression for R reduces to

$$R_\infty = \exp(-\tfrac{1}{5}R_0^2\gamma^2G^2\delta^2), \tag{43}$$

a result which closely resembles the exact asymptotic result of Tanner and Stejskal (1968). To this extent the gaussian phase assumption has some accidental justification for spherical geometry. The dependence of R on observation time Δ has been examined by Packer and Rees (1972) using oil/water emulsions. Their data for water in oil is shown in Fig. 15 where the asymptotic independence of R on Δ is clearly apparent.

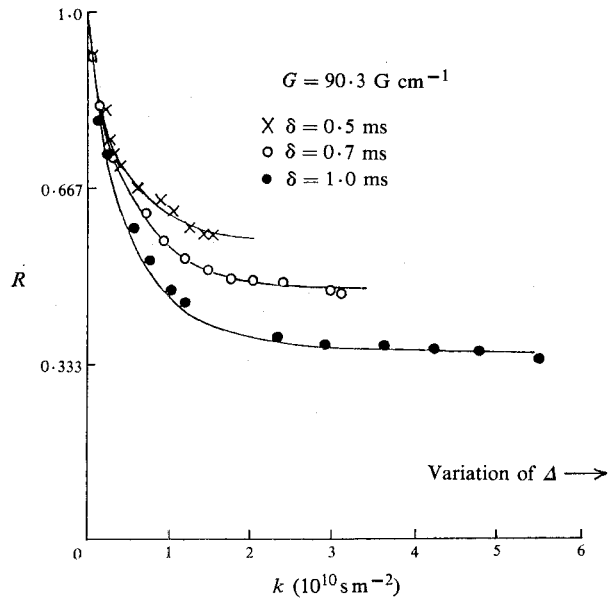

Fig. 15. Echo attenuation data of Packer and Rees (1972) for water protons in water/oil emulsion. Note the lack of a common dependence on k where restricted diffusion is apparent. As the observational timescale is increased sufficiently the data exhibit an independence of R from Δ characteristic of molecular confinement. The theoretical curves are fits for droplet size distributions.

PFGNMR has proven accurate and convenient in measuring droplet size distributions for oil/water emulsions and for fat droplets in cream and cheese (Callaghan *et al.* 1983*a*). The scale of barrier dimensions to which the method is sensitive makes it a useful biophysical tool, with an advantage over electron or optical microscopy in that it is non-invasive and highly penetrating. Both the laminar and spherical geometry restricted diffusion models have been applied to appropriate problems involving diffusion within plant and animal cell walls (Tanner and Stejskal 1968; Cooper *et al.* 1974; Packer and Sellwood 1978).

(*c*) *Diffusion near an Attractive Centre*

The phenomenon of particles diffusing in an isotropic medium but subject to a harmonic potential has been treated in detail by Stejskal (1965) in the case where the restoring force is balanced by frictional damping. The terminal velocity of the particle is then

$$\dot{\boldsymbol{r}} = -\beta \boldsymbol{r}, \tag{44}$$

with β the ratio of the force constant to the friction coefficient. For such particles it may be shown that

$$P_s(\boldsymbol{r}_0 \mid \boldsymbol{r}, t) = [2\pi D\{1-\exp(-2\beta t)\}/\beta]^{-3/2} \times \exp[-\beta\{\boldsymbol{r} - \boldsymbol{r}_0 \exp(-\beta t)\}^2/2D\{1-\exp(-2\beta t)\}], \tag{45}$$

$$P_0(\boldsymbol{r}_0) = (2\pi D/\beta)^{-3/2} \exp(-\beta r_0^2/2D). \tag{46}$$

Then we have

$$R = \exp[-\gamma^2\delta^2 G^2 D\{1-\exp(-\beta\Delta)\}/\beta]. \tag{47}$$

An example of such diffusion is found in polymer gels where the network has bulk modulus E and friction coefficient Φ per unit volume. It has been shown by de Gennes (1976) that for longitudinal gel fluctuations of wavevector κ, the elastic restoring force per unit volume is given by

$$\boldsymbol{F}_{el} = -E\kappa^2 \boldsymbol{r}, \tag{48}$$

so that $\beta = E\kappa^2/\Phi$ for this system.

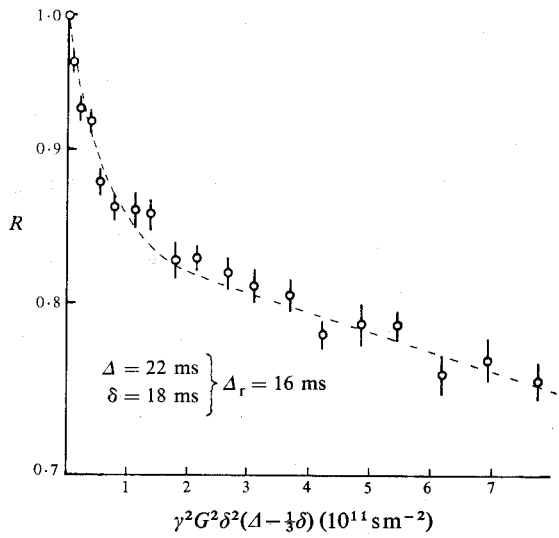

Fig. 16. Echo attenuation plot for an 8% solution of 2×10^6 daltons polystyrene in carbon tetrachloride for $\Delta < T_r$. The fast component is identified with cooperative diffusion.

A PFGNMR experiment has been performed by Callaghan and Pinder (1980) on an entangled polystyrene solution of sufficiently high molar mass that the experimental timescale could be made short compared with the entanglement lifetime T_r. For such an experiment the semi-dilute solution forms a quasi-permanent network and PFGNMR measures network displacements on a scale larger than the polymer dimensions. A nonlinear dependence of $\ln R$ on G^2 is apparent as shown in Fig. 16. The rapid component is attributed to disturbances of long wavelength ($\kappa^2 \ll E\Delta/\Phi$) and yields an effective gel cooperative diffusion coefficient, $D_c = E/\Phi$, which scales with polymer concentration c according to the de Gennes (1976) cooperative law

$$D_c \sim c^{0.75}. \tag{49}$$

(d) Curvilinear Diffusion

Despite the constraining tube formed by impeding neighbouring coils, the random coil polymer in semi-dilute solution has an asymptotic diffusion which is three-dimensional and isotropic. This is because the tube renews itself on average every reptation period T_r. It is this branching option which bestows the attribute of a random walk. On a timescale shorter than T_r, however, the polymer is truly confined and, while the diffusion is Brownian along the one-dimensional curvilinear tube coordinates, this behaviour appears non-Brownian in the laboratory frame. This

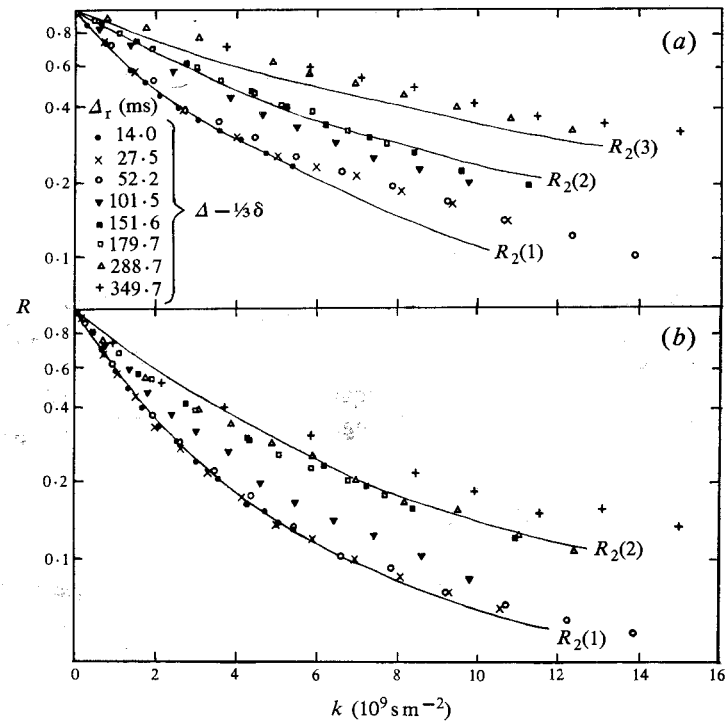

Fig. 17. Echo attenuation plots for a 24·8% sample of Aerosol OT/water for (*a*) an equilibrated sample and (*b*) a sample with three days equilibration. Results show the dependence of diffusive behaviour as Δ is varied over a wide range. For spins residing in one domain only, the data should be coincident. The theoretical curves (equation 53) for the cases where the spins sample successively one, two and then higher numbers of domains are shown with D values obtained by fitting $\Delta = 15$ ms data in the case $N = 1$.

non-Brownian self-diffusion could be detected by a technique sensitive to displacements on a scale smaller than the polymer dimensions. A similar phenomenon is apparent in liquid crystals over observation times sufficient for the molecules to traverse several domains. Here the molecules are compelled to travel in the curvilinear path defined by the phase layer to which they belong, although here the curvilinear paths may be two-dimensional (e.g. water in lamellar amphiphile structures).

In a PFGNMR experiment, curvilinear diffusion is manifested as restricted diffusion with a characteristic dependence of R on Δ. Let us consider motion confined to one- or two-dimensional elements oriented randomly. We define a total r.m.s. curvilinear path length Λ (without branches) comprised of N elements of r.m.s. length λ, migration along this path occurring in a diffusion time t. For the example of two-dimensional motion we have

$$\Lambda^2 = 4Dt, \tag{50}$$

$$\Lambda = N\lambda. \tag{51}$$

For N large, the laboratory frame displacements are characterized by

$$\overline{(r^2)}^{\frac{1}{2}} = N^{\frac{1}{2}}\lambda = (4DN^{-1}t)^{\frac{1}{2}} = \lambda^{\frac{1}{2}}(4Dt)^{\frac{1}{4}}. \tag{52}$$

While the distribution of laboratory frame displacements is gaussian, the dependence of their r.m.s. value on $t^{\frac{1}{4}}$ rather than $t^{\frac{1}{2}}$ is distinctly non-Brownian. Such $t^{\frac{1}{4}}$ dependence was predicted by de Gennes (1971) for one-dimensional polymer diffusion on a timescale $t < T_r$. In PFGNMR the gaussian displacement distribution leads to a linear dependence of ln R on $G^2\delta^2$ but with a slope decreasing as $\Delta_r^{\frac{1}{2}}$. An interesting example of such non-Brownian behaviour is provided by the case of water diffusion in poly-domain lyotropic liquid crystals as the diffusive timescale is increased sufficiently for the water molecules to traverse more than one domain. Fig. 17 shows echo attenuation plots by Callaghan and Soderman (1983) for lamellar Aerosol OT/water as Δ is varied. The data show that as Δ increases the curvature characteristic of randomly oriented single-domain diffusion (equation 34) disappears, the data exhibiting a more linear gaussian dependence at longer observation times. In this case of finite N, the appropriately modified echo attenuation is given as

$$R_2(N) = \exp(-kDN^{-1}) \int_0^1 \exp(kDN^{-1}x^2)\, dx. \tag{53}$$

The data of Fig. 17 suggest that the water molecules on average migrate respectively across one, two or three domains as the observational timescale increases.

6. Flow

In each of the examples considered so far, the average molecular displacement has been zero and the ensemble phase average $\overline{\exp(i\phi_D)}$ real. Under conditions of flow, a term $-\nabla . \boldsymbol{v}P_s$ must be added to the right-hand side of equation (29) and the solution to the phase average will contain, in addition to amplitude decay, a factor corresponding to the phase shift. Stejskal (1965) has shown, for a particle of velocity $\boldsymbol{v}$ and diffusion tensor $\mathbf{D}$, that the narrow pulse expression for the echo attenuation may be written as

$$R = \exp(-\gamma^2\delta^2 \boldsymbol{G}.\mathbf{D}.\boldsymbol{G}\Delta - i\gamma\delta \boldsymbol{G}.\boldsymbol{v}\Delta). \tag{54}$$

Hayward *et al.* (1972) have investigated the echo attenuations, in the presence of both pulsed and steady gradients, of two simple flow patterns, namely plug flow and laminar flow. Allowing that the effects of diffusion and flow are separable, these authors showed that the in-phase component in the echo amplitude contains an extra factor under conditions of flow as follows:

(i) For plug flow, i.e. $P(v) = \delta(v)$ where $P(v)$ is the probability density for velocity v along the gradient axis, they found

$$\mathscr{R}(R) = \cos\{\gamma v(G\delta\Delta + G_0\tau^2)\}. \tag{55}$$

(ii) For laminar flow in a circular pipe of radius R_0, i.e. $P(v) = 1/2\bar{v}$ and $v(r) = K(R_0^2 - r^2)$, they found

$$\mathscr{R}(R) = \sin\{2\gamma\bar{v}(G\delta\Delta + G_0\tau^2)\}/2\gamma\bar{v}(G\delta\Delta + G_0\tau^2). \tag{56}$$

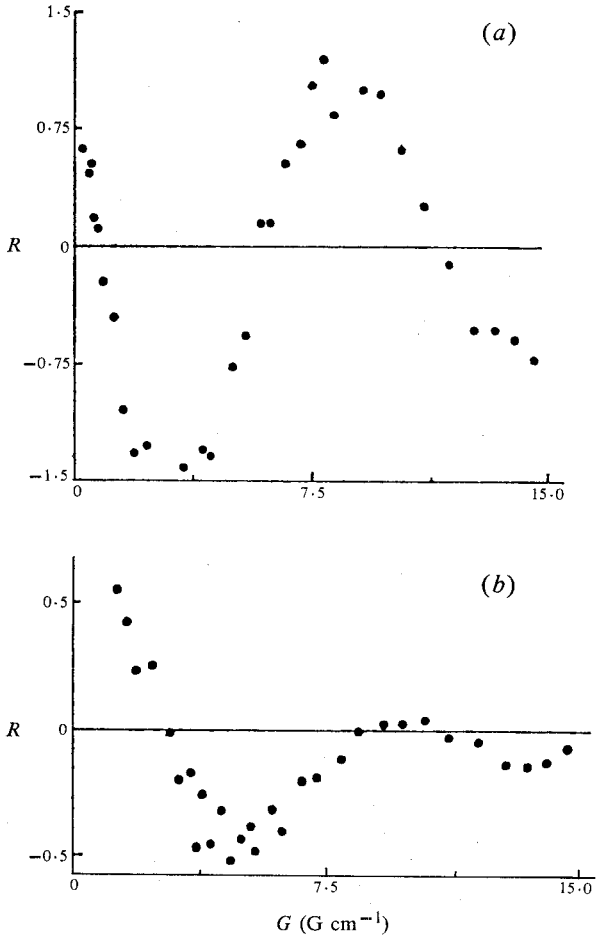

Fig. 18. Variation of echo attenuation at 2τ with and without field gradient pulses for a sample of (*a*) 0·3% agar/water gel moving with average velocity 2·8 cm s^{-1} through a circular pipe of diameter 0·5 cm; (*b*) 0·1% agar/water gel moving at 0·7 cm s^{-1} through the same pipe ($\delta = 0{\cdot}97$ ms, $\Delta = 29$ ms).

Both these flow expressions oscillate with the field gradient amplitude G, whereas diffusion only induces echo decay. In an elegant experiment on agar gel, Hayward *et al.* (1972) demonstrated behaviour predicted by equations (55) and (56) by comparing the echo amplitude with and without gradient pulses for concentrated gel where plug flow is expected (Fig. 18*a*) and for dilute gel for which laminar conditions apply (Fig. 18*b*). The data exhibit the characteristic oscillatory behaviour of cosine and sinc functions respectively.

Despite the pioneering work of these authors, the PFGNMR method has not been exploited in flow investigations, despite its potential to examine the behaviour of complex systems such as non-Newtonian fluids. Again, the temporal resolution

offered by the technique would enable measurement of flow patterns over differing timescales in the millisecond regime and could thus prove a sensitive probe of fluid turbulence and relaxation phenomena.

The medical implications of such flow dependent effects are considerable. Where spin-echoes are employed in NMR imaging experiments, echo phase shifts may be used as a signature for material in transport. As an example, the mapped proton spin densities from water molecules moving in blood capillaries could be distinguished from that of water trapped within the cells of tissue.

7. Tensor Interactions

If the spin Hamiltonian contains spin tensors of rank greater than 1, the Hahn-echo sequence is unable to refocus the consequent spectral broadening, and effective T_2 values are reduced. Such terms may arise due to secular elements of the spin–spin dipolar interactions or, for $j > \frac{1}{2}$ (for example deuterium), the quadrupolar interaction with the electric field gradients associated with the molecular orbitals. These interactions are of special concern in PFGNMR experiments on liquid crystals where dipolar or quadrupolar broadening is not averaged to zero by molecular motion as is the case in isotropic liquids, or by chemical exchange as is the case for protons in water molecules.

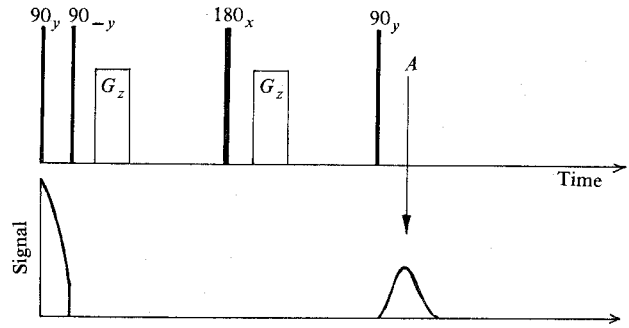

Fig. 19. The r.f. gradient pulse sequence for a PFGNMR experiment using tensor polarization. The two initial 90° pulses produce a state of two-quantum coherence in which the Zeeman precessions are doubled for the gradient pulses shown. The final 90° pulse causes the magnetic polarization to be recalled under the influence of the tensor interaction.

It is useful to consider second rank tensors which transform as the Legendre polynomial, $\frac{1}{2}(3\cos^2\Theta - 1)$. Because of this transformation property, the associated broadening can be minimized by orienting a sample so that the domain directors assume the magic angle of 54·74° to the laboratory magnetic field. Such an approach has been used by Roeder *et al.* (1976) in measuring the self-diffusion coefficient of oriented potassium oleate in the lamellar phase.

Tensor interactions may also be refocused by using appropriate r.f. pulses. In particular, the solid-echo sequence $\theta_1|_y = \theta_2|_x = 90°$ refocuses the entire rank 2 quadrupole and dipole Hamiltonian components but onyl half the residual Zeeman broadening. Recourse to equations (2) and (4) shows that the Stejskal–Tanner equation for the echo attenuation still applies for such a pulse sequence in the presence

of these interactions. Where higher order tensor terms are to be removed it is necessary to turn to multiple r.f. pulse sequences. In a sophisticated experiment, Blinc *et al.* (1973) have superposed a rapid multiple 90° r.f. sequence (Ostroff and Waugh 1966), a pulsed magnetic field gradient sequence and a slow Carr–Purcell train of r.f. pulses in order to remove proton dipolar interactions in nematic MBBA. The effective T_2 was thus increased from 100 μs to nearly 100 ms, enabling spin-echo observation over a sufficient timescale for a self-diffusion coefficient to be obtained.

In fact the existence of tensor interactions may be turned to advantage in the PFGNMR experiment. In particular, a pulse sequence in which spin polarization is transformed to a state of 'two quantum coherence' is described in Fig. 19. The density matrix following the second 90° pulse contains mostly rank 2 tensor components which commute with the dipole or quadrupole Hamiltonian but precess at twice the Larmor frequency about the z-axis Zeeman fields. On regeneration of the $\overline{\langle J_x + iJ_y \rangle}$ polarization following the final 90° pulse, an echo results. Because of the dependence of the echo attenuation on the square of the Larmor precession frequency, the resulting attenuation has four times greater sensitivity to diffusion than an experiment employing entirely vector polarization.

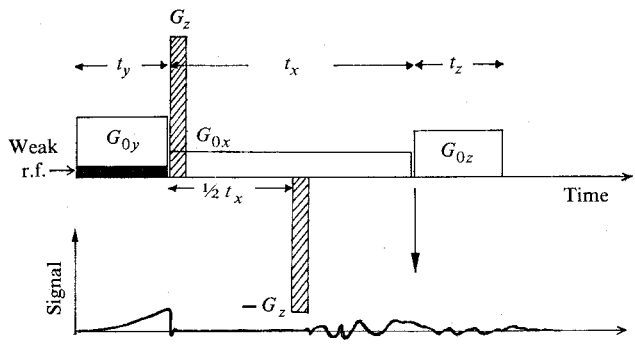

Fig. 20. Combined imaging/PFGNMR experiment in which the local spin-echo amplitude (resolved by the imaging sequence) is varied under the influence of the strong gradient pulses G_z and $-G_z$. Note that gradient pulse inversion is required if an echo is to be produced from G_z while the precessions in the weak steady imaging field gradient G_{0x} are unperturbed.

8. Conclusions

It is apparent that pulsed field gradient NMR can in principle reveal the wavevector and frequency spectrum of the displacement self-correlation function $P_s(\boldsymbol{r}_0 \mid \boldsymbol{r}, t)$. Equation (7) shows, however, that this spectrum is averaged over the static spin distribution $P_0(\boldsymbol{r}_0)$ and in consequence the PFGNMR results are difficult to interpret where $P_0(\boldsymbol{r}_0)$ is non-uniform, as may well be the case in highly disperse phases or biological tissue. Considerable simplification can be achieved if specific NMR sensitive nuclei (e.g. ^{2}H) are used to label local regions of the phase, but such labelling is unavoidably difficult in practice.

An alternative approach is to resolve the static spin distribution by NMR imaging (Mansfield and Morris 1982) in which $P_0(\boldsymbol{r}_0)$ is directly mapped by analysis of the nuclear Larmor frequency distribution in the presence of steady magnetic field gradients. It is conceivable that the imaging and PFG experiments might be superposed

as shown in Fig. 20. Here the imaging method is that of Fourier Zeugmatography (Kumar *et al.* 1975). Three successive orthogonal gradients are used to resolve the spin distribution. A narrow-band r.f. pulse selects a slice of spins normal to the y-axis and subsequent free induction decays are digitized along the time coordinate t_z with a matrix of such signals being obtained by varying the parameter t_x (or G_x). Fourier transformation along the rows and columns of this matrix produces $P_0(\boldsymbol{r}_0)$ in the selected slice of x–z plane. By analysing the variation of local signal intensities under an additional PFG, the dependence of $P_s(\boldsymbol{r}_0 \mid \boldsymbol{r}, t)$ on each of $\boldsymbol{r}$, t and $\boldsymbol{r}_0$ may in principle be revealed. While this experiment is undoubtedly ambitious, it is feasible given the capacity of modern processing technology.

Note that the resolution with which $P_s(\boldsymbol{r}_0 \mid \boldsymbol{r}, t)$ may currently be determined is some two to three orders of magnitude greater than that possible in the measurement of $P_0(\boldsymbol{r}_0)$. In obtaining the static spin distribution, the Zeugmatography method relies on the absolute Larmor frequencies which are spuriously broadened by chemical shifts and homogeneity imperfections. Furthermore, because Zeugmatography requires data acquisition in the presence of field gradients, it suffers from the limitations imposed by spectrometer bandwidth. In contrast, PFGNMR constitutes a differential spectroscopy in which the frequency spread of interest is singularly isolated without inhomogeneous broadening and with a resolution limited only by the Heisenberg natural linewidth. This fundamental limit is in fact several orders of magnitude smaller than the resolution currently achieved. At present the technique is limited solely by the production of large magnetic field gradients with experimental assemblies sufficiently rigid to prevent spurious sample movement. With appropriately improved technology PFGNMR could achieve a resolution of a few Ångströms. It might then complement neutron scattering as an investigative tool in the truly microscopic domain.

References

Abragam, A. (1961). 'Principles of Nuclear Magnetism' (Oxford Univ. Press).

Blinc, R., Burgar, M., Luzar, M., Pirs, J., Zupancic, I., and Zumer, S. (1974). *Phys. Rev. Lett.* **33**, 1192.

Blinc, R., Pirs, J., and Zupancic, I. (1973). *Phys. Rev. Lett.* **30**, 546.

Boden, N., Corne, S. A., and Jolley, K. W. (1984). *Chem. Phys. Lett.* **105**, 99.

Callaghan, P. T., Jolley, K. W., and Humphrey, R. S. (1983*a*). *J. Colloid Interface Sci.* **83**, 521.

Callaghan, P. T., Jolley, K. W., and Lelievre, J. (1979). *Biophys. J.* **28**, 133.

Callaghan, P. T., Jolley, K. W., and Trotter, C. M. (1980*a*). *J. Magn. Reson.* **39**, 525.

Callaghan, P. T., Le Gros, M. A., and Pinder, D. N. (1983*b*). *J. Chem. Phys.* **79**, 6372.

Callaghan, P. T., and Lelievre, J. (1984). The size and shape of amylopectin: a study using pulsed field gradient nuclear magnetic resonance. *Biopolymers* (in press).

Callaghan, P. T., and Pinder, D. N. (1980). *Macromolecules* **13**, 1085.

Callaghan, P. T., and Pinder, D. N. (1981). *Macromolecules* **14**, 1334.

Callaghan, P. T., and Pinder, D. N. (1984). *Macromolecules* **17**, 431.

Callaghan, P. T., and Soderman, O. (1983). *J. Phys. Chem.* **87**, 1737.

Callaghan, P. T., Trotter, C. M., and Jolley, K. W. (1980*b*). *J. Magn. Reson.* **37**, 247.

Carr, H. Y., and Purcell, E. M. (1954). *Phys. Rev.* **94**, 630.

Clark, M. E., Burnell, E. E., Chapman, N. R., and Hinke, J. A. M. (1982). *Biophys. J.* **39**, 289.

Cooper, R. L., Chang, D. B., Young, A. C., Martin, C. J., and Anker-Johnson, B. (1974). *Biophys J.* **14**, 161.

de Gennes, P. G. (1971). *J. Chem. Phys.* **55**, 572.

de Gennes, P. G. (1976). *Macromolecules* **9**, 587, 598.

Derbyshire, W., and Duff, I. D. (1973). *Faraday Discuss. Chem. Soc.* **57**, 243.

Flory, P. (1971). 'Principles of Polymer Chemistry' (Cornell Univ. Press).

Fukushima, E., and Roeder, S. B. W. (1981). 'Experimental Pulse NMR' (Addison–Wesley: Reading, Mass.).
Gordon, R. E., and Strange, J. H. (1978). *J. Phys.* C **11**, 3213.
Hahn, E. L. (1950). *Phys. Rev.* **80**, 580.
Hayter, J. B., Hecht, A. M., White, J. W., and Tiddy, G. J. T. (1974). *Faraday Discuss. Chem. Soc.* **57**, 130.
Hayward, R. J., Packer, K. J., and Tomlinson, D. J. (1972). *Mol. Phys.* **23**, 1083.
James, T. L., and McDonald, G. G. (1973). *J. Magn. Reson.* **11**, 58.
Kumar, A., Welti, D., and Ernst, R. R. (1975). *J. Magn. Reson.* **18**, 69.
Lindman, B., Stilbs, P., and Moseley, M. E. (1981). *J. Colloid Interface Sci.* **83**, 569.
McCall, D. W., Douglass, D. C., and Anderson, E. W. (1963). *Ber. Bunsenges. Phys. Chem.* **67**, 336.
Mansfield, P., and Morris, P. G. (1982). 'NMR Imaging in Biomedicine' (Ed. J. S. Waugh), Suppl. 2, *Adv. Magn. Reson.* (Academic: New York).
Meiboom, S., and Gill, D. (1959). *Rev. Scient. Instrum.* **29**, 688.
Mills, R. (1973). *J. Phys. Chem.* **77**, 687.
Murday, J. S., and Cotts, R. M. (1968). *J. Chem. Phys.* **48**, 4938.
Murday, J. S., and Cotts, R. M. (1970). *J. Chem. Phys.* **53**, 4724.
Ostroff, E. D., and Waugh, J. S. (1966). *Phys. Rev. Lett.* **16**, 1097.
Packer, K. J., and Rees, C. (1972). *J. Colloid Interface Sci.* **40**, 206.
Packer, K. J., and Sellwood, T. C. (1978). *J. Chem. Soc.* **74**, 1592.
Pouyet, G., Francois, J., Dayantis, J., and Weill, G. (1980). *Macromolecules* **14**, 176.
Roeder, S. B. W., Burnell, E. E., Kuo, A., and Wade, C. G. (1976). *J. Chem. Phys.* **64**, 1848.
Schick, A. F., and Singer, S. J. (1950). *J. Phys. Chem.* **54**, 1028.
Stejskal, E. O. (1965). *J. Chem. Phys.* **43**, 3597.
Stejskal, E. O., and Tanner, J. E. (1965). *J. Chem. Phys.* **42**, 288.
Tanner, J. E. (1965). *Rev. Scient. Instrum.* **36**, 1086.
Tanner, J. E. (1970). *J. Chem. Phys.* **52**, 2523.
Tanner, J. E. (1978). *J. Chem. Phys.* **69**, 1748.
Tanner, J. E., and Stejskal, E. O. (1968). *J. Chem. Phys.* **49**, 1768.
Torrey, H. C. (1956). *Phys. Rev.* **104**, 563.
Wang, J. H. (1954). *J. Am. Chem. Soc.* **76**, 4755.
Webster, D. S., and Marsden, K. H. (1974). *Rev. Scient. Instrum.* **45**, 1232.
Weill, G., and des Cloizeaux, J. (1979). *J. Phys.* (*Paris*) **40**, 99.
Williams, W. D., Seymour, E. F. W., and Cotts, R. M. (1978). *J. Magn. Reson.* **31**, 271.
Yamakawa, H. (1968). *J. Chem. Phys.* **36**, 2995.
Yamakawa, H. (1971). 'Modern Theory of Polymer Solutions' (Harper and Row: New York).
Zupancic, I., Pirs, J., Luzar, M., Blinc, R., and Doane, J. W. (1974). *Solid State Commun.* **15**, 227.

Manuscript received 16 February, accepted 16 April 1984